Supplementary Information

3D printing of resilient, lightweight and conductive MXene/reduced graphene oxide architectures for broadband electromagnetic interference shielding

Yang Dai,[a] Hao-Bin Zhang,[a]* Xinyu Wu,[a] Lulu Li,[a] Yu Zhang,[b] Zhiming Deng,[b] Zhong-Zhen Yu[a,b]

[a] State Key Laboratory of Organic-Inorganic Composites, College of Materials Science and Engineering, Beijing University of Chemical Technology, Beijing 100029, China

[b] Beijing Key Laboratory of Advanced Functional Polymer Composites, Beijing University of Chemical Technology, Beijing, 100029, China

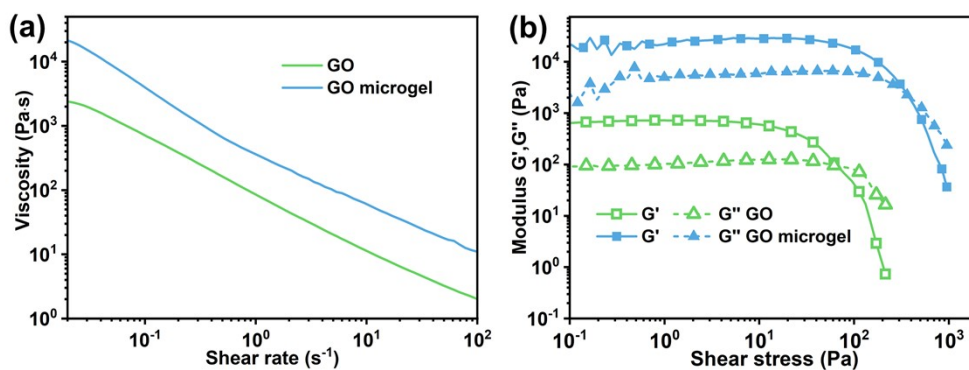E-mail: zhanghaobin@buct.edu.cn (H.-B. Zhang)

Fig. S1. (a) The viscosity and (b) storage modulus (G') and loss modulus (G") of GO suspension and GO microgel with a GO content of 2.5 wt%.
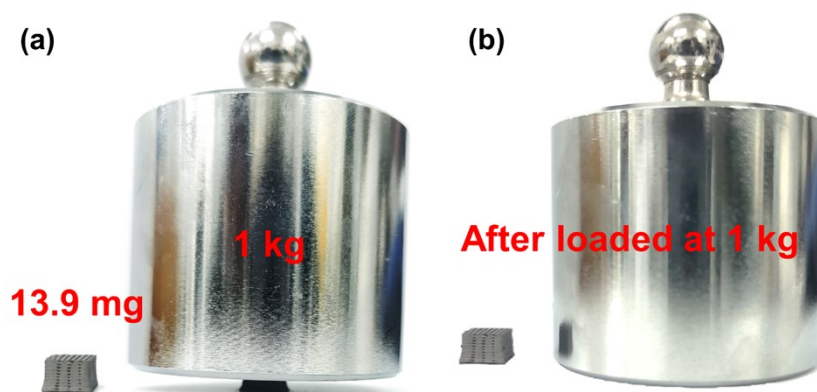

Fig. S2. The digital photos of printed scaffolds (a) loaded and (b) unloaded with 1kg.
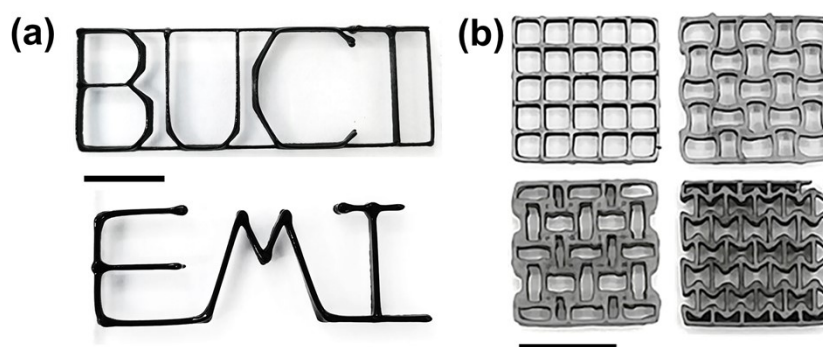

Fig. S3. The digital photos of printed patterns of (a) letters "BUCT" and "EMI" for 4 layers, (b) the different periodic structures of frame structure, curved concave polygon structure, four tangential antichiral structure and concave hexagon structure, the scale of the digital photos is 1 cm.
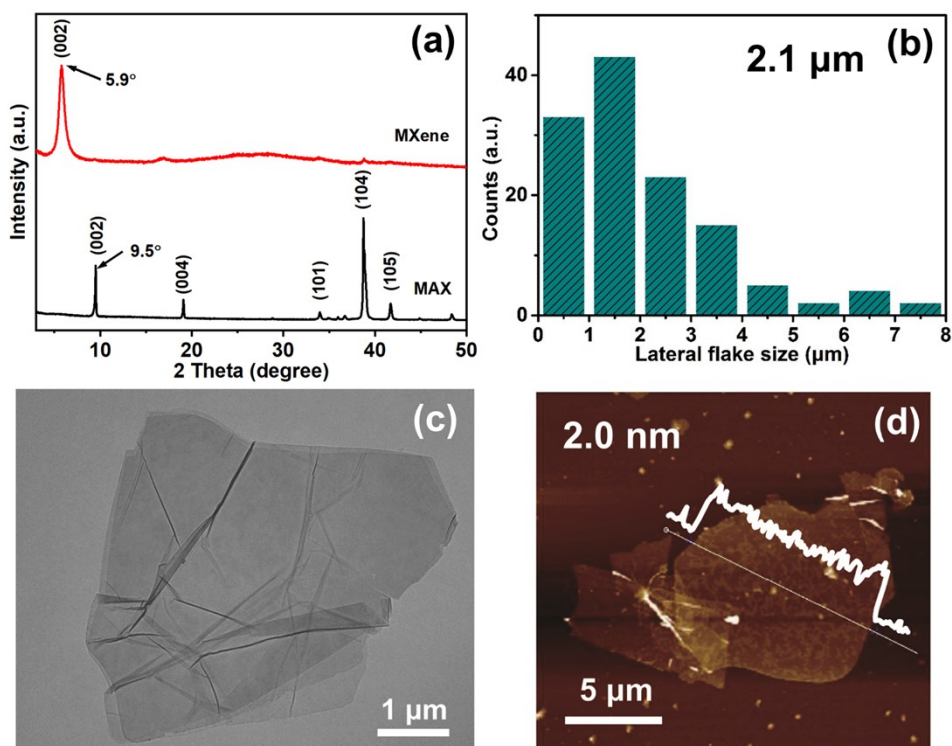
Fig. S4. The characteristic of MXene nanosheets. (a) XRD patterns of MAX and few-layered Ti$_3$C$_2$T$_x$ MXene, (b) the histogram of lateral sizes of MXene flakes based on SEM images of diluted MXene suspension. (c) TEM image and (d) AFM image of MXene flakes.

The characteristic peaks (104) and (105) of Ti$_3$AlC$_2$ almost disappear, and the significantly strengthened peak (002) shifts from 9.5° to 5.9°, corresponding to the layer spacing increasing from 9.2 Å to 15.2 Å (Figure S4a).
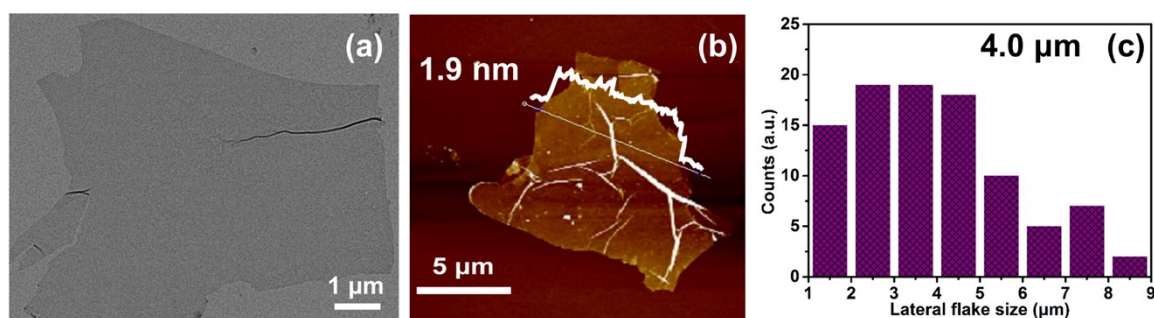

Fig. S5. The characteristic of GO nanosheets. (a) TEM image of GO, (b) AFM image of GO sheets, (c) histogram of lateral sizes of GO sheets on the basis of SEM images of diluted GO suspension.
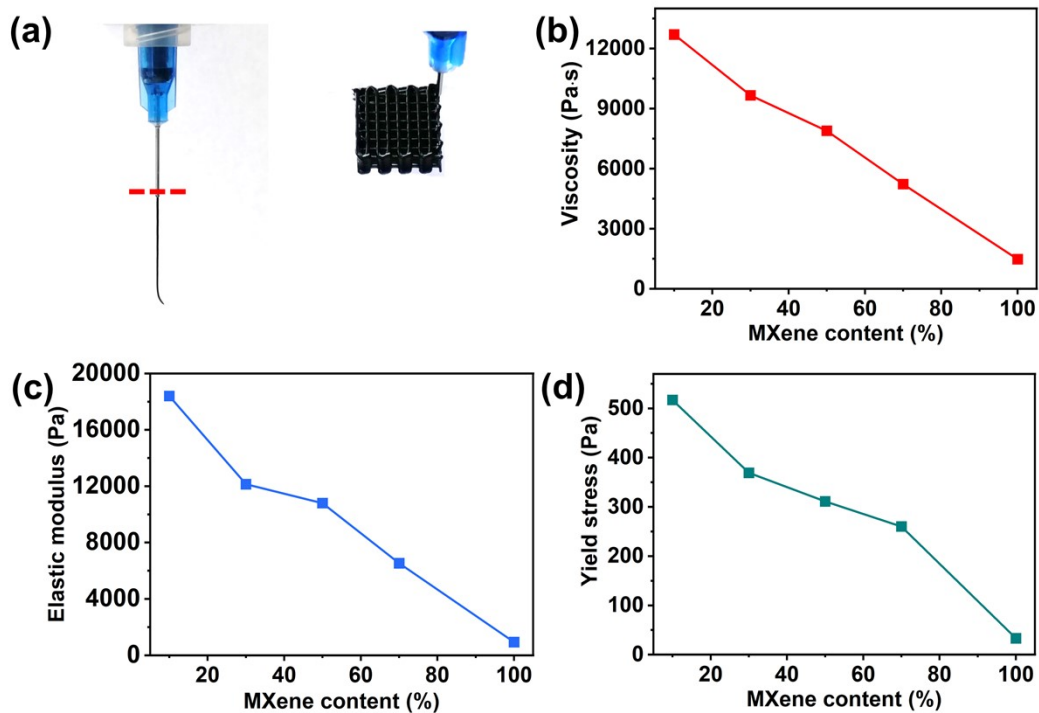
Fig. S6. (a) Photographs of the MXene/GO ink extruded from the needle and free-standing on the substrate. The values of (b) shear viscosity and (c) the elastic modulus (G') and (d) yield stress of the MXene/GO ink with different MXene contents.
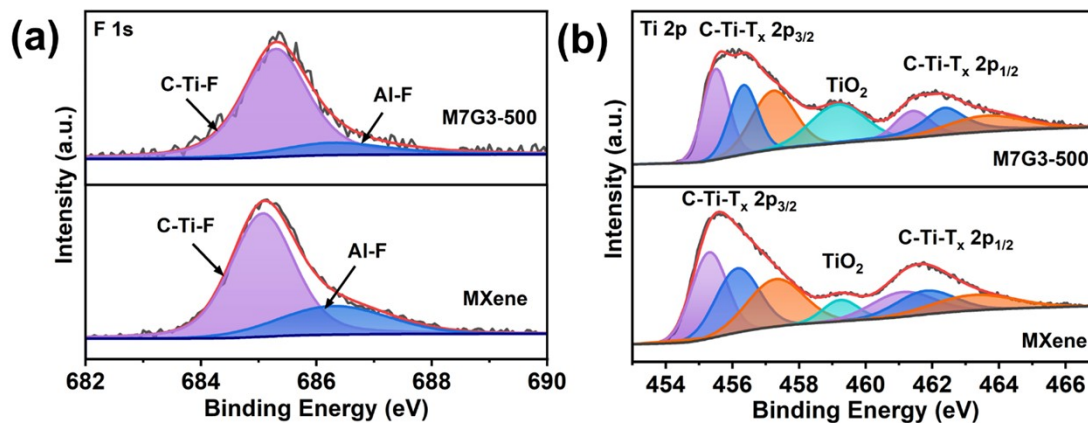
Fig. S7. The (a) F 1s and (b)Ti 2p spectra of MXene and M7G3-500.
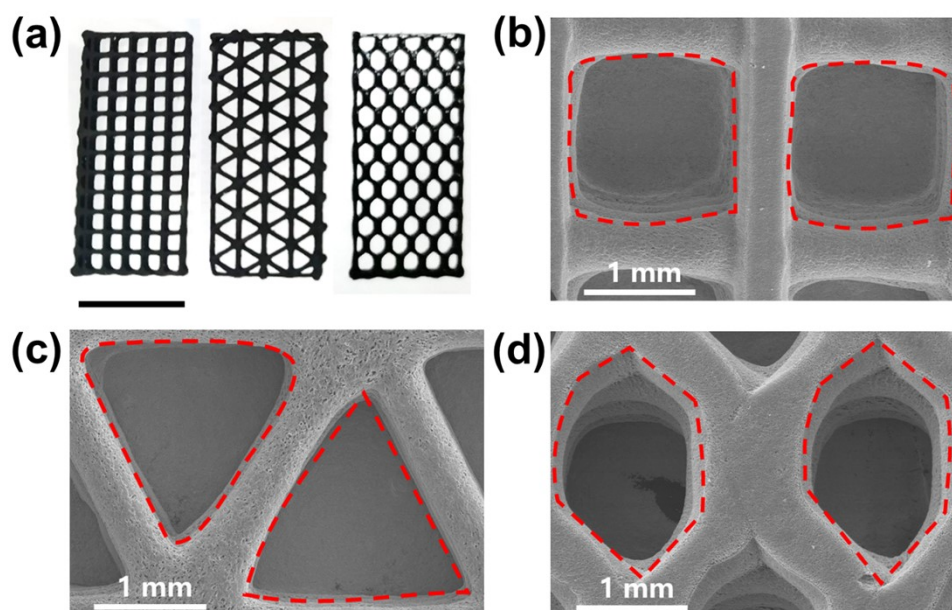
Fig. S8. (a) The photograph and SEM images in the top view of the MXene/RGO scaffolds with different cell geometries: (b) square, (c) triangle, (d) hexagon.
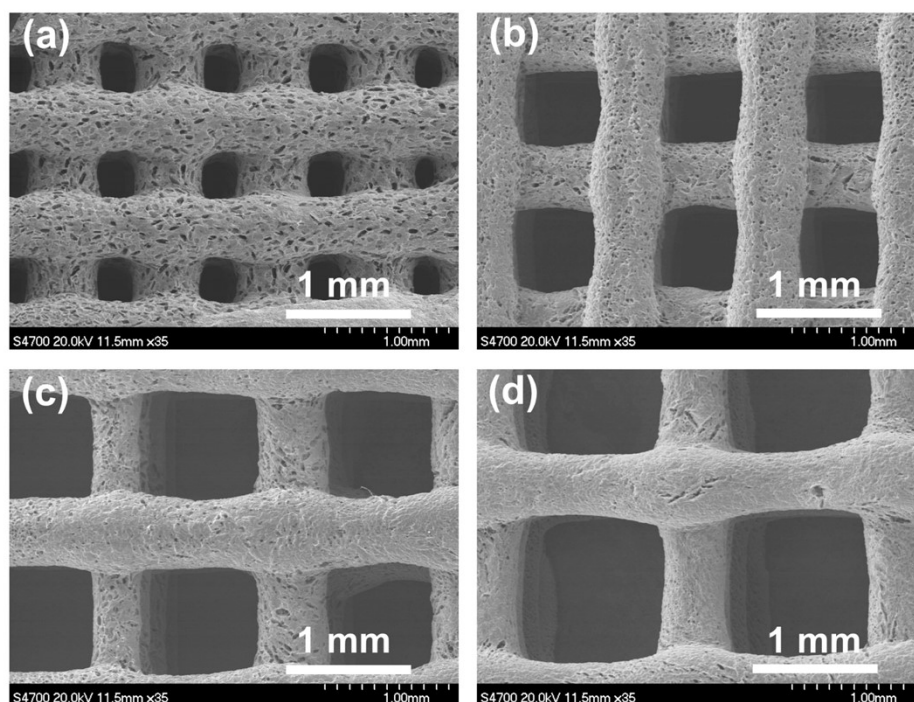
Fig. S9. The SEM images of M7G3-500 with filament spacings of: (a) 0.9 mm, (b) 1.2 mm, (c) 1.5 mm, (d) 1.8 mm.
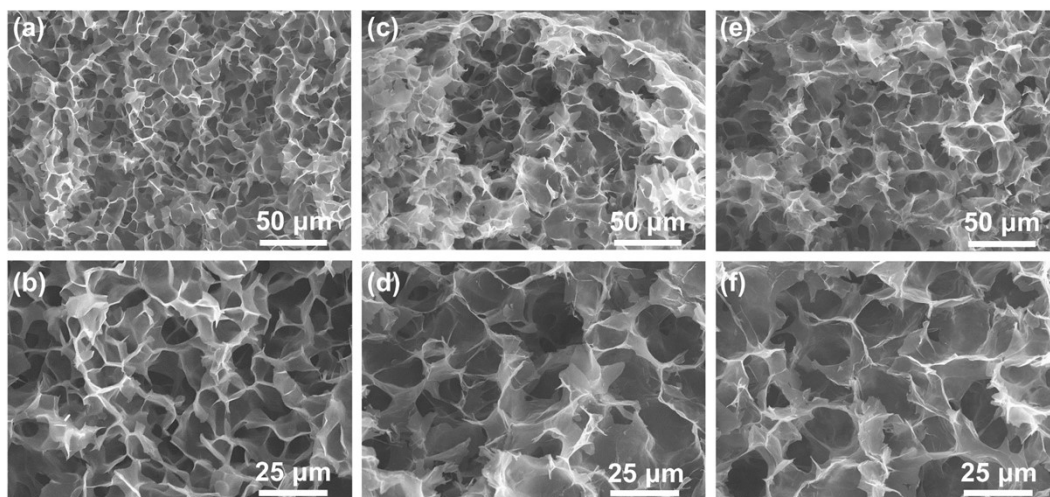
Fig. S10. The SEM images in the cross-sectional view of (a, b) M1G1, (c, d) M1G1-80, (e, f) M1G1-500.
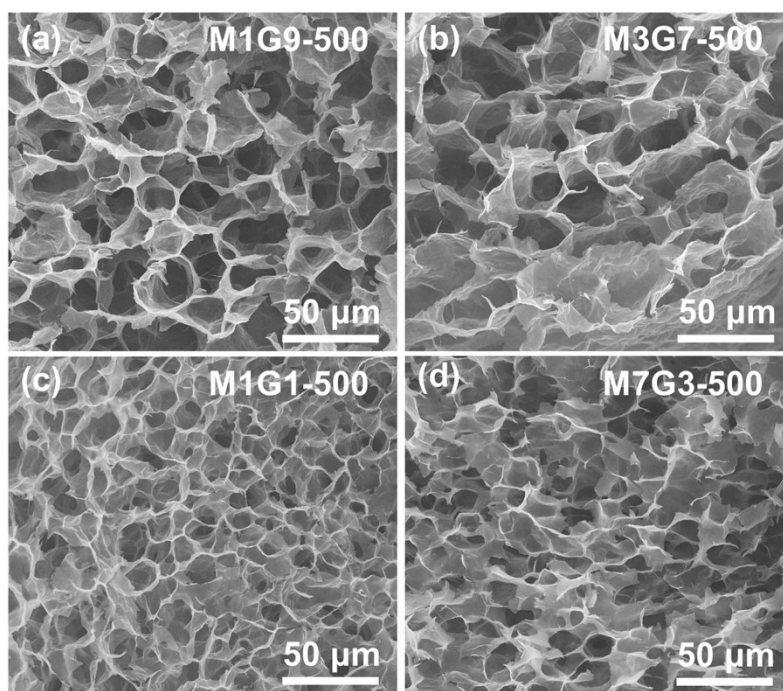
Fig. S11. The SEM images in cross-sectional view of (a) M1G9-500, (b) M3G7-500, (c) M1G1-50, (d) M7G3-500.
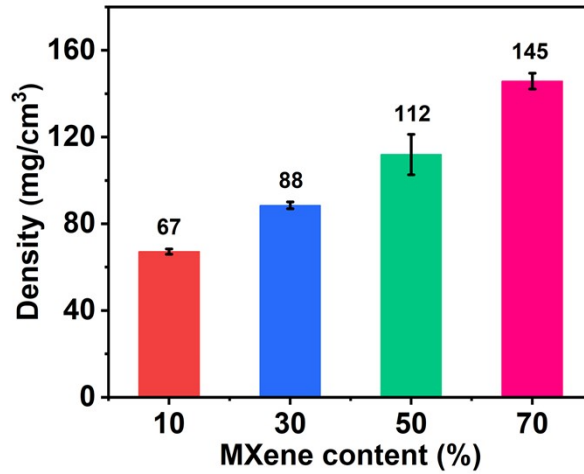
Fig. S12. The densities of MXene/RGO filaments with different MXene contents.
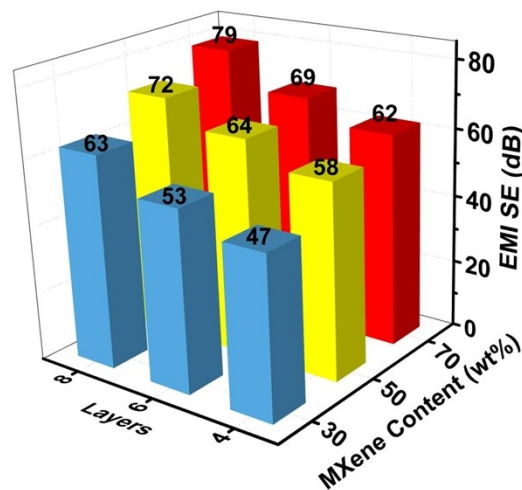
Fig. S13. The EMI SE values of the MXene/RGO scaffolds versus the MXene contents and the number of printed layers.
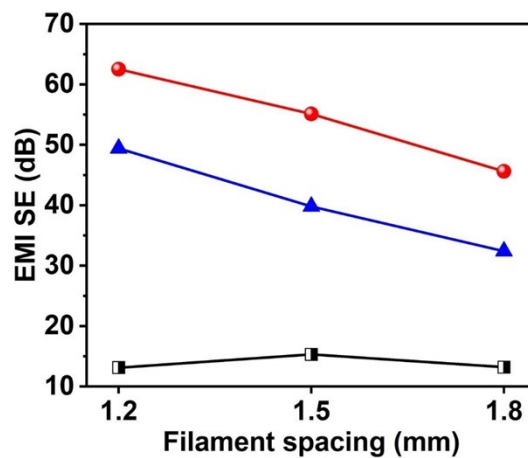
Fig. S14. The EMI SE values of M7G3-500 with different filament spacings in X-band.
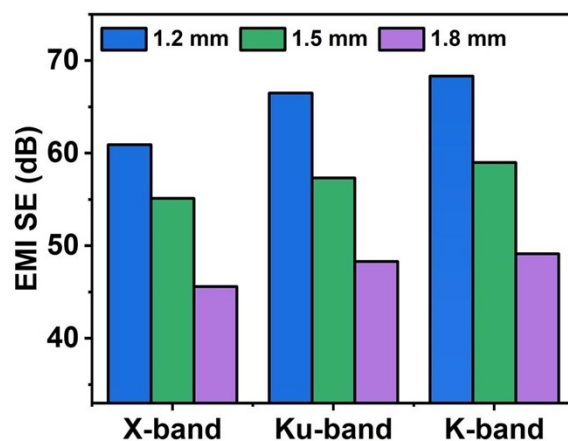
Fig. S15. The EMI SE values of M7G3-500 with different filament spacings in X-band, Ku-band, and K-band.

Straight-through structure **Staggered structure**
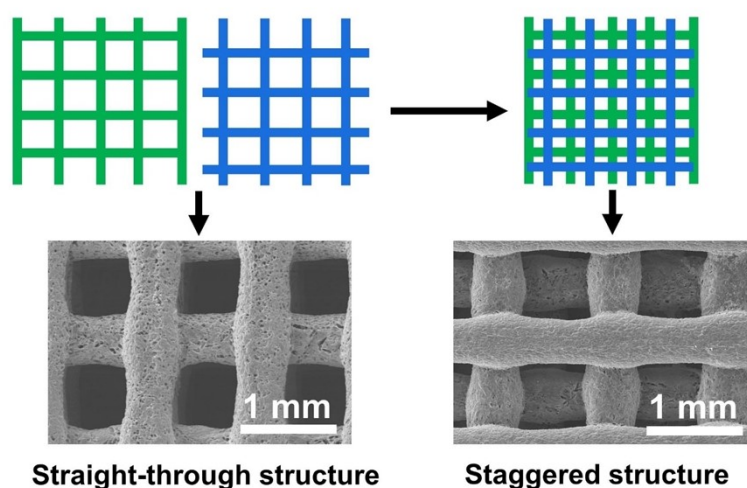
Fig. S16. Schematic and SEM images show the straight-through and staggered structure for M7G3-500.
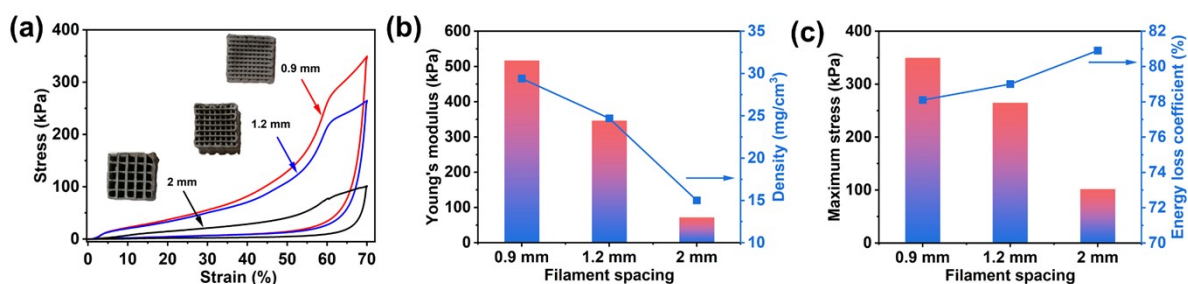
Fig. S17. (a) Compressive stress-strain curves, (b) Young's modulus and densities, and (c) the

maximum stresses and energy loss coefficients of M1G9-500 with the different filament spacings of 0.9 mm, 1.2 mm and 2 mm at 70% compression.
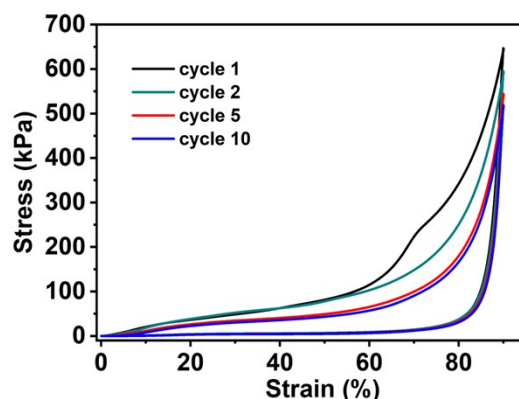
Fig. S18. The cyclic compression performance of M1G9-500 at 90% strain for 10 cycles.
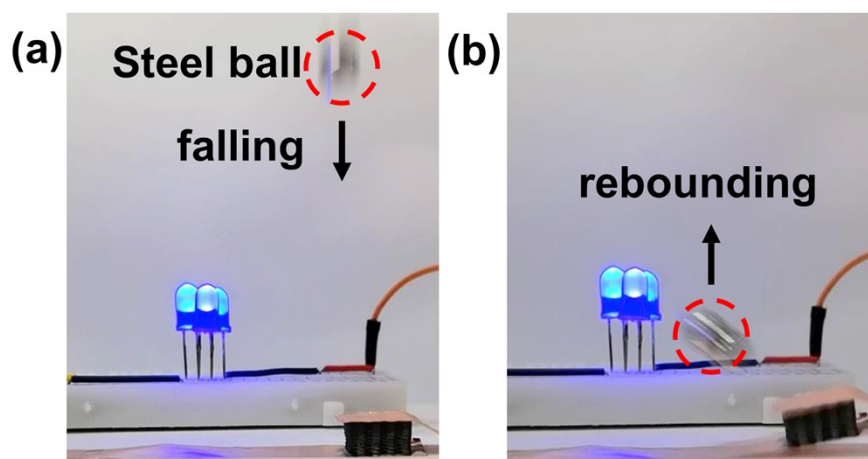
Fig. S19. The photographs of impact process of the MXene/RGO scaffold: (a) before and (b) after impacted by a steel ball (0.8 g). In the impact process, the LEDs maintain the similar brightness, indicating the robust structure with the anti-impacting protection property.

Table S1. The ink constituent of the printable MXene/GO ink.

Samples	MXene mass (mg)	GO mass (mg)	AA mass (mg)	MXene-10% Mass (g)	GO-2.5% Mass (g)	Filler content (%)
M1G9	10	90	180	0.1	3.6	2.7
M3G7	30	70	140	0.3	2.8	3.2

M1G1	50	50	100	0.5	2.5	4.0	
M7G3	70	30	60	0.7	1.2	5.3	

Table S2. Preparation methods and EMI shielding performance of typical 3D printed materials in 8.2-12.4 GHz.

Materials	Method	Electrical conductivity (S/m)	EMI SE (dB)	Thickness (mm)	Density (g/cm^3)	SE/t (dB/mm)	SSE/t (dB cm^2.g^{-1})	Ref
CNT/CB/ ABS	FDM	1	16	2	/	8	/	[1]
PLA/ graphene	FDM	4	16	1.2	/	13.3	/	[2]
CNT/PLA	FDM	20	67.5	2.0	/	33.8	/	[3]
CNT/PLA	FDM	5000	30	0.7	0.4	42.9	214.3	[4]
Ag @ CNF/ PLA	FDM	2.1×10^5	46	~0.7	~2	65.7	328.6	[5]
PE/ graphene	FDM	/	29	2.05	0.44	2.05	318.0	[6]
PLA/GNPs/CNTs	FDM	82	36.8	2	/	18.4	/	[7]
PVA/GNP	FDM	3.6	31.7	2.43	/	13.0	/	[8]
PLA/GNP	FDM	30	34.7	2	/	17.4		[9]
Fe$_3$O$_4$ /GMFs/HPC	FFF	580	57.19	1.05	/	54.5	/	[10]
Liquid metal/ elastomer	DIW	~ 3.4×10^6 (EGaIn)	82	9.5	~ 6.4 (EGaIn)	8.63	/	[11]
CNT/CS	DIW	4.1	25.0	3	0.072	8.3	1157.4	[12]
Graphene/ PDMS	DIW	50	45	4.8	/	9.4	/	[13]
MG frame	DIW	5323	76.2	2	0.105	38.10	3628.6	[14]
MXene/PEO	DIW	/	23	0.101	/	227.7	/	[15]
MXene/PEDOT :PSS	DIW	1525.8	51.7	0.295	/	175.3	/	[16]
MXene/RGO scaffold	DIW	73	37.0	1.2	0.016	30.8	19270.8	**This work**
		357	47.4	1.2	0.029	39.5	13620.7	
		771	57.5	1.2	0.033	47.9	14520.2	
		1013	62.5	1.4	0.038	44.6	11748.1	

1013	68.8	2.2	0.043	31.3	7272.7
1013	79.3	2.7	0.051	29.4	5758.9

Table S3. The EMI shielding performance of the MXene/RGO scaffolds.

(A) The effect of filament spacings in X-band, Ku-band, and K-band

Spacing (mm)	Frequency (GHz)	Thickness (mm)	EMI SE (dB)
1.2		1.36	62.5
1.5	8.2-12.4	1.35	55.1
1.8		1.30	45.6
1.2		1.23	66.5
1.5	12.4-18	1.21	57.4
1.8		1.23	48.3
1.2		1.20	68.3
1.5	18-26.5	1.29	59.0
1.8		1.22	49.1

(B) The effect of stacking styles

Samples	Thickness (mm)	EMI SE (dB)
4L	1.36	62.5
S-4L	1.42	67.7
S-6L	2.01	75.7
S-8L	2.63	80.5

(C) The effect of Zigzag structure

Samples	Thickness (mm)	EMI SE (dB)
Z3	2.96	65.9
Z5	2.32	71.2
Z8	2.11	82.0

Table S4. The summary mechanical performance of the MXene/RGO scaffolds with different MXene content at 50% compression.

MXene content (%)	Density (mg/cm^3)	Young's modulus (MPa)	Maximum strength (kPa)	Plastic deformation (%)
10	24.7	0.463	214.3	0.5
30	37.9	0.636	358.6	3.1

50	44.0	1.002	414.2	29.4	
70	52.4	3.423	430.8	35.9	

Table S5. The survey of the ink composition and mechanical performance of 3D printed materials.

Ink composition	Density (mg/cm^3)	Compressive strain (%)	Maximum Strength (kPa)	Cycles	Stress retention (%)	Ref
GO + Urea	47	30	15	5	95	[17]
GO + CaCl$_2$	10	80	90	10	75.3	[18]
GO + resin	43.8	/	/	/	/	[19]
GO + CNT+ Ni(OH)$_2$	132.5	60	156.7	10	79.9	[20]
GO	10	50	83.6	10	70.6	[21]
GO + Silica	53	50	1194	10	37.5	[22]
MXene	15.69	10	0.98	50	88.8	[23]
MXene + NiCoP	/	/	/	/	/	[24]
MXene + ZnSO$_4$	/	/	/	/	/	[25]
MXene+ GO+CNT	/	/	/	/	/	[26]
MXene	21.3	/	/	/	/	[27]
MXene + GO	24.7	90	646.8	10	80.1	**This work**

References

1. D. P. Schmitz, L. G. Ecco, S. Dul, E. C. L. Pereira, B. G. Soares, G. M. O. Barra and A. Pegoretti, *Mater. Today Commun.*, 2018, **15**, 70-80.

2. K. Prashantha and F. Roger, *J. Macromol. Sci. A*, 2017, **54**, 24-29.

3. Y. Wang, Z. Fan , H. Zhang, J. Guo, D.-X. Yan, S. Wang, K.Dai, Z.-M. Li, *Mater. Des.*, 2021, **197**, 109222.

4. K. Chizari, M. Arjmand, Z. Liu, U. Sundararaj and D. Therriault, *Mater. Today Commun.*, 2017, **11**, 112-118.

5. H. Wei, X. Cauchy, I. O. Navas, Y. Abderrafai, K. Chizari, U. Sundararaj, Y. Liu, J. Leng and D. Therriault, *ACS Appl. Mater. Interfaces*, 2019, **11**, 24523-24532.

6. J. Jing, Y. Xiong, S. Shi, H. Pei, Y. Chen and P. Lambin, *Compos. Sci. Technol.*, 2021, **207**, 108732.

7. S. Shi, Z. Peng, J. Jing, L. Yang and Y. Chen, *ACS Sustainable Chem. Eng.*, 2020, **8**, 7962-7972.

8. L. Yang, Y. Chen, M. Wang, S. Shi and J. Jing, *Ind. Eng. Chem. Res.*, 2020, **59**, 8066-8077.

9. S. Shi, Z. Peng, J. Jing, L. Yang, Y. Chen, R. Kotsilkova and E. Ivanov, *Ind. Eng. Chem. Res.*, 2020,

59, 15565-15575.

10. M. Wajahat, J. H. Kim, J. Ahn, S. Lee, J. Bae, J. Pyo and S. K. Seol, *Carbon*, 2020, **167**, 278-284.

11. Z. Wang, J. Ren, R. Liu, X. Sun, D. Huang, W. Xu, J. Jiang, K. Ma and Y. Liu, *Compos. Part A Appl. Sci. Manuf.*, 2020, **136**, 105957.

12. X. Pei, M. Zhao, R. Li, H. Lu, R. Yu, Z. Xu, D. Li, Y. Tang and W. Xing, *Compos. Part A Appl. Sci. Manuf.*, 2021, **145**, 106363.

13. Z. Wang, W. Yang, R. Liu, X. Zhang, H. Nie and Y. Liu, *Compos. Sci. Technol.*, 2021, **206**, 108652.

14. X. Wu, T. Tu, Y. Dai, P. Tang, Y. Zhang, Z. Deng, L. Li, H.-B. Zhang and Z.-Z. Yu, *Nano-Micro Lett.*, 2021, **13**, 148.

15. S. Y. Hong, Y. Sun, J. Lee, M. Yifei, M. Wang, J.-D. Nam and J. Suhr, *Polymer*, 2021, **236**, 124312.

16. J. Liu, L. McKeon, J. Garcia, S. Pinilla, S. Barwich, M. Mobius, P. Stamenov, J. N. Coleman and V. Nicolosi, *Adv. Mater.*, 2022, **34**, 2106253.

17. X. Tang, H. Zhou, Z. Cai, D. Cheng, P. He, P. Xie, D. Zhang and T. Fan, *ACS Nano*, 2018, **12**, 3502-3511.

18. Y. Jiang, Z. Xu, T. Huang, Y. Liu, F. Guo, J. Xi, W. Gao, and C. Gao, *Adv. Funct. Mater.*, 2018, **28**, 1707024.

19. R. M. Hensleigh, H. Cui, J. S. Oakdale, J. C. Ye, P. G. Campbell, E. B. Duoss, C. M. Spadaccini, X. Zheng and M. A. Worsley, *Mater. Horiz.*, 2018, **5**, 1035-1041.

20. D. Kong, Y. Wang, S. Huang, B. Zhang, Y. V. Lim, G. J. Sim, Y. A. P. Valdivia, Q. Ge and H. Y. Yang, *ACS Nano*, 2020, **14**, 9675-9686.

21. Q. Zhang, F. Zhang, S. P. Medarametla, H. Li, C. Zhou and D. Lin, *Small*, 2016, **12**, 1702-1708.

22. C. Zhu, T. Y. Han, E. B. Duoss, A. M. Golobic, J. D. Kuntz, C. M. Spadaccini and M. A. Worsley, *Nat. Commun.*, 2015, **6**, 6962.

23. H. Tetik, J. Orangi, G. Yang, K. Zhao, S. Bin Mujib, G. Singh, M. Beidaghi and D. Lin, *Adv. Mater.*, 2022, **34**, 2104980.

24. L. Yu, W. Li, C. Wei, Q. Yang, Y. Shao and J. Sun, *Nano-Micro Lett.*, 2020, **12**, 143.

25. Z. Fan, J. Jin, C. Li, J. Cai, C. Wei, Y. Shao, G. Zou and J. Sun, *ACS Nano*, 2021, **15**, 3098-3107.

26. Z. Fan, C. Wei, L. Yu, Z. Xia, J. Cai, Z. Tian, G. Zou, S. X. Dou and J. Sun, *ACS Nano*, 2020, **14**, 867-876.

27. C. Yang, X. Wu, H. Xia, J. Zhou, Y. Wu, R. Yang, G. Zhou and L. Qiu, *ACS Nano*, 2022, **16**, 2699-2710.